Nanoscale

COMMUNICATION

View Article Online
View Journal | View Issue

Cite this: *Nanoscale*, 2017, **9**, 18609

Received 23rd August 2017,
Accepted 12th November 2017

DOI: 10.1039/c7nr06291e

rsc.li/nanoscale

The Yin and Yang of coordinating co-solvents in the size-tuning of Fe_3O_4 nanocrystals through flow synthesis†

Mingxia Jiao,[a] Lihong Jing,[b] Xiaojun Wei,[b] Chunyan Liu,[b] Xiliang Luo *[a] and Mingyuan Gao *[b]

The present study reports a continuous flow synthesis of differently sized Fe_3O_4 nanocrystals stabilized by oleylamine and oleic acid. Oleylamine and oleic acid are particularly investigated to elucidate their roles in tailoring the size and magnetic properties of the resulting particles potentially useful for magnetic resonance imaging.

Superparamagnetic iron oxide nanoparticles have been widely applied in biomedical fields, especially as contrast agents in magnetic resonance imaging (MRI).[1–5] Driven by these appealing applications, precise control over the particle size of iron oxide nanoparticles has been intensively investigated in the past few decades,[6–8] due to the strong size-related superparamagnetism of magnetic iron oxide nanoparticles and pharmacokinetic behaviors as well.[9,10]

Differently sized iron oxide nanocrystals with high crystallinity were commonly achievable through thermal decomposition synthesis by varying different reaction parameters.[8,11–13] For example, tuning the reaction time can vary the particle size in a certain range, which, however, is sometimes accompanied by broadening of the particle size distribution due to Ostwald ripening.[14] Surface ligand is in fact indispensable in the wet-chemical synthesis of high quality nanoparticles, not only for increasing the mutual compatibility between the particle cores and the dispersion media, but also for preventing the particles from uncontrolled growth.[10,15,16] Tuning the ratio of the surface ligand to the precursor can also lead to differently sized iron oxide nanoparticles, *e.g.*, 7–28 nm Fe_3O_4 nanocrystals were prepared by increasing the ratio of oleic acid to ferric oleate from 0.1 : 1 to 3 : 1.[17] However, when the ligand-to-precursor ratio is high enough, the commonly used ligands such as oleylamine (OM) and oleic acid (OA) will inevitably change the solvent properties, and thus may heavily affect the formation process of nanoparticles. But it remains barely touched upon in the literature.

Despite the remarkable achievements in the size-controlled synthesis of iron oxide nanoparticles, previous studies were mainly based on conventional batch reactions.[8,11,12] The following practical applications will suffer from the poor batch-to-batch reproducibility.[14,18,19] Fortunately, a newly developed flow chemistry method offers a potential solution to the large scale synthesis of nanocrystals owing to its automated continuous synthetic conditions.[14,20,21] Semiconductor nanocrystals are the most representative inorganic nanocrystals achievable through the continuous flow synthesis. The effects of reaction parameters on the particle size and further on the optical properties have been intensively studied over the past decade.[22–25] Nevertheless, there remains a lack of systematic study about the effects of ligands on the solvent properties of the reaction system, and further on the size of the resulting nanocrystals. Such a study would undoubtedly push the development of the flow synthesis for obtaining differently sized and monodisperse iron oxide nanoparticles for biomedical applications.

On the basis of our previous investigations on the continuous flow synthesis of Fe_3O_4 nanoparticles and $NaGdF_4$:Yb,Er nanocrystals,[14,18] herein, we report the flow synthesis of Fe_3O_4 nanocrystals with the particle size in the range of 3–9 nm, which is obtained by varying the concentration of ligands including OM, OA, and alcohols bearing a long alkyl chain. The coordinating effect and the co-solvent effect of OM and OA are discussed in details from the point of view of particle nucleation and growth kinetics and thermodynamics.

In brief, Fe_3O_4 nanocrystals were continuously synthesized using a tube reactor with an inner diameter of 1.0 mm at 250 °C under a pressure of 30 bar, with a computer-controlled automatic synthesis system. The continuous synthesis is schematically shown in Scheme 1. The residence time was set as 3 min, which is apparently shorter than that (30 min) for batch reactions because of the significantly enhanced heat transfer rate.[10] Typically, 2.0 mmol ferric acetylacetonate was

---

[a] *Key Laboratory of Sensor Analysis of Tumor Marker, Ministry of Education, College of Chemistry and Molecular Engineering, Qingdao University of Science and Technology, Qingdao 266042, China. E-mail: xiliangluo@qust.edu.cn*

[b] *Institute of Chemistry, Chinese Academy of Sciences, Bei Yi Jie 2, Zhong Guan Cun, Beijing 100190, China. E-mail: gaomy@iccas.ac.cn*

† Electronic supplementary information (ESI) available: (1) Experimental details, (2) characterization of the flow synthesized Fe_3O_4 nanocrystals, (3) analysis of the diffusion coefficient. See DOI: 10.1039/c7nr06291e

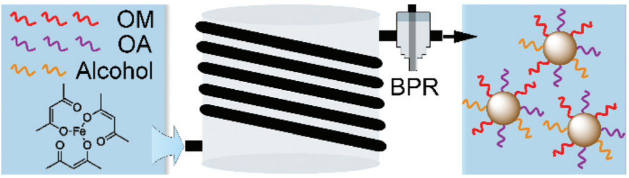

Scheme 1 Sketch of the flow synthesis of Fe_3O_4 nanocrystals. BPR represents a back pressure regulator.

pyrolyzed in the presence of 10.0 mmol 1-octadecanol, 6.0 mmol (0.3 M) OM and 6.0 mmol (0.3 M) OA in 20 mL anisole (boiling point of 154 °C) which was used as a solvent under the high pressure to facilitate the purification process.[14] Stabilized by OM and OA *via* the amine and carboxylate, respectively, as confirmed by Fourier transform infrared (FTIR) spectroscopy shown in Fig. S1 in the ESI,† the resulting nanocrystals were readily dispersed in organic solvents such as cyclohexane. The TEM image of the as-prepared Fe_3O_4 nanocrystals is shown in Fig. 1a. The average particle size is 4.2 nm, and the relative standard deviation (RSD) calculated from the corresponding histogram (Fig. S2a, ESI†) is 14.3%.

The magnetic properties of Fe_3O_4 nanocrystals are known to strongly depend on the particle size.[26,27] Since different surface ligands have different effects on the nucleation and growth processes of nanocrystals, the concentrations of OM and OA were set equal and adjusted simultaneously throughout the experiments for investigating the concentration effect of the OM/OA pair. When increasing the concentration of OM/OA from 0.3 M up to 0.6 M, the average particle size was increased from 4.2 nm to 8.2 nm as shown in Fig. 1b. The Fe_3O_4 nanocrystals obtained are rather monodisperse with the RSD value slightly down to 13.4% (Fig. S2c, ESI†). However, upon further increase of the concentration of OM/OA to 1.2 M, the average particle size decreased to 6.0 nm as shown in Fig. 1c, while the RSD drops to 10.0% (Fig. S2b, ESI†). The powder X-ray diffraction (XRD) patterns of the as-prepared nanocrystals shown in Fig. 1d match well with that for magnetite (JCPDS card no. 86-0866). The enhanced intensity and the narrowed peak width of the main diffraction peaks from 4.2 nm to 8.2 nm samples support the increased crystallinity and the particle size as well.

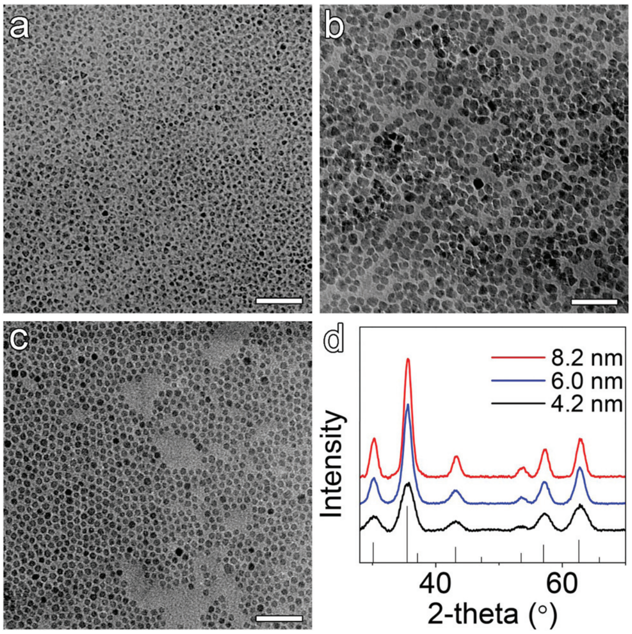

Fig. 1 Transmission electron microscopy (TEM) images of Fe_3O_4 nanocrystals prepared in the presence of 1-octadecanol and different concentrations of OM/OA, respectively: (a) 0.3 M, (b) 0.6 M, (c) 1.2 M (the scale bars correspond to 50 nm), and powder X-ray diffraction (XRD) patterns (d) of the as-prepared nanocrystals together with the line pattern for magnetite according to the JCPDS card (86-0866).

To exclude any dilution effect caused by the introduction of OM/OA on the particle size, an equal volume of anisole was added instead of OM/OA into the initial stock solution. The nanocrystals obtained under the same preparative conditions, as displayed in Fig. S3 (ESI†), are nearly identical to those shown in Fig. 1a. Therefore, the effective size increase induced by increasing the concentration of OM/OA can be attributed to the effect of surface ligands. During the particle formation process, ligands coordinate to the nanocrystal surface to prevent particle aggregation, otherwise uncontrolled growth occurs when the ligands are insufficient (0.15 M OM/OA) as displayed in Fig. S4 (ESI†). On the other hand, ligands can also coordinate with the Fe monomer, which can change its reactivity.[17] When the concentration of OM/OA was increased from 0.3 M to 0.6 M, the reactivity of the monomer was reduced due to the stronger binding effect. In consequence, the supersaturation degree of the reaction system would decrease, which is then favourable for growing larger particles out of the reaction system, from the thermodynamics aspect, due to the reduced number of nuclei generated during the nucleation process.

Apart from acting as surface ligands, OM and OA at some point start to induce non-ignorable change to the solvent properties of the reaction system. For example, when the concentration of OM/OA reached 1.2 M, the viscosity of the reaction system for obtaining 6.0 nm particles ($V_{OM+OA}:V_{anisole} = 1:1.3$) is of 7.3 mPa s at 20 °C, much higher than that (3.0 mPa s) of the system producing 8.2 nm particles ($V_{OM+OA}:V_{anisole} = 1:2.6$). According to Einstein's formula (ESI†), the diffusion coefficient of the solute is inversely correlated with the viscosity of the solvent. In consequence of the increased viscosity of the solvent, the nanocrystal growth rate will be decreased and smaller particles are generated.[18]

Apart from the concentration effects of OM and OA on the solvent properties, long alkyl chain alcohols also influence the nucleation process as they participate in the generation of the monomer by acting as a reducing agent.[6] As shown in Fig. S5,† in the presence of 0.6 M OM/OA, replacing 1-octadecanol with 1,2-dodecanediol can decrease the particle size from 8.2 ± 1.1 nm down to 3.0 ± 0.3 nm, while the particle size can be increased from 8.2 ± 1.1 nm to 8.6 ± 1.2 nm in the absence of alcohol. The presence of multiple hydroxyl groups leads to a higher supersaturation degree for the monomer, thus resulting in smaller nanocrystals.

To explore the application of the flow-synthesized Fe_3O_4 nanocrystals as MRI contrast agents, differently sized Fe_3O_4 nanocrystals (4.2 nm, 6.0 nm, and 8.2 nm) obtained above were rendered water-soluble and biocompatible upon ligand exchange, by replacing the OM and OA ligands with a polyethylene glycol (M_w = 2000) ligand bearing a catechol group. The hydrodynamic properties of the resultant PEGylated Fe_3O_4 nanoparticles were carefully examined by *Z*-average, which is intensity-weighted and more sensitive to the presence of larger particles. As shown in Fig. 2a, the particles, irrespective of the core size, remain colloidally stable over one month, which makes them reliable for *in vivo* applications. The MRI contrast enhancement effects of the PEGylated Fe_3O_4 nanoparticles acquired at 3.0 T are shown in Fig. 2b. In brief, all these particles show significant T_1 and T_2 effects, and thus can potentially be used as dual-modal T_1/T_2 contrast agents. As expected, the T_1 effect decreases against the particle size, while the T_2 effect presents an opposite tendency. By linear regression fitting of the experimental data shown in Fig. S6 (ESI†), the molar relaxivity r_1 of the 4.2 nm, 6.0 nm, and 8.2 nm nanoparticles is of 7.9 mM^{-1} s^{-1}, 5.6 mM^{-1} s^{-1}, and 4.2 mM^{-1} s^{-1}, and r_2 is of 71.8 mM^{-1} s^{-1}, 83.1 mM^{-1} s^{-1}, and 121.3 mM^{-1} s^{-1}, respectively. Notably, the 4.2 nm particles simultaneously exhibit higher r_1 and r_2 than the literature data for similarly sized Fe_3O_4 nanoparticles synthesized through batch preparation,[10,12] which may be attributed to the extraordinary experimental conditions especially the high pressure of the reaction system.

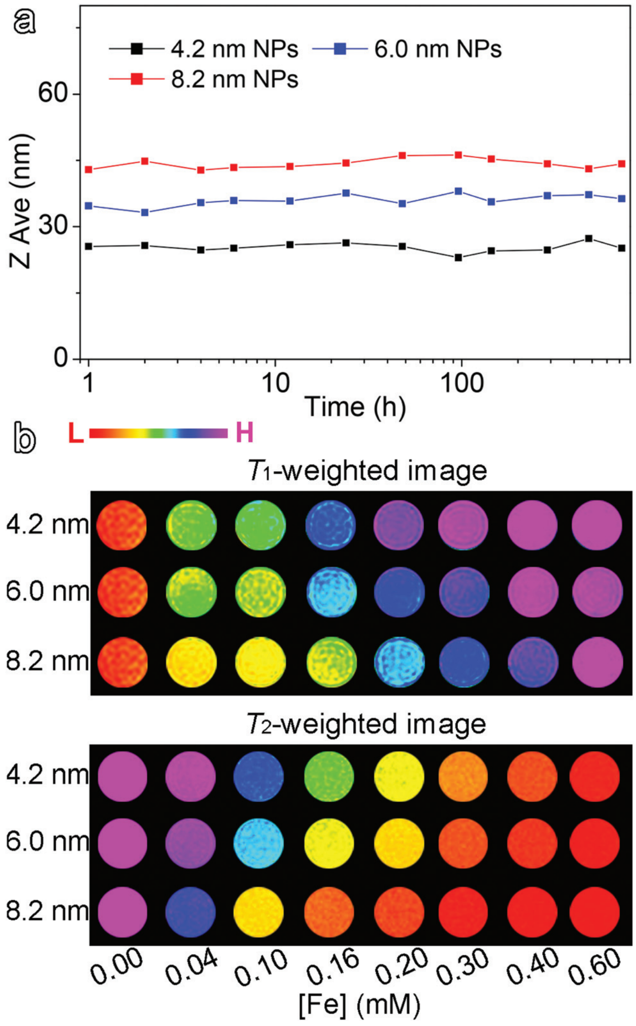

Fig. 2 Temporal evolution of the hydrodynamic sizes of PEGylated Fe_3O_4 nanoparticles in water (a), together with color-coded T_1-weighted and T_2-weighted MR images of aqueous solutions containing Fe_3O_4 nanoparticles with different Fe concentrations (b).

Conclusions

In summary, it is demonstrated that the concentration effects of OM and OA ligands on the size of Fe_3O_4 nanoparticles obtained through continuous flow synthesis have two sides. On one hand, increasing the ligand concentration is in favour of the formation of larger particles due to the decreased supersaturation degree of monomers bound to the ligands. On the other hand, the simultaneously increased viscosity in consequence of high enough ligand concentration favors the formation of smaller particles owing to the lowered diffusion coefficient. The opposite size-tuning effects from the coordinating OM/OA co-solvent pair are the interplay of "Yin and Yang" when it comes to their effect as a function of concentration, which describes the unity of opposites in nature. By properly adjusting the concentration of OM/OA, the size of monodisperse Fe_3O_4 nanocrystals in the range of 4.2–8.2 nm is successfully tuned. Moreover, long alkyl chain alcohols also play a role in size tunability. The presence of polyalcohol can decrease the bottom size further down to 3.0 nm, while excluding the alcohol can increase the top size up to 8.6 nm. The relaxometric studies on the flow-synthesized Fe_3O_4 nanoparticles reveal that the above particles exhibit extraordinarily higher longitudinal and transversal relaxivities in comparison with those of similarly sized Fe_3O_4 nanocrystals bearing an identical surface capping structure. In conclusion, the current investigations have paved an effective and reliable approach for achieving high performance MRI contrast agents with potentially scaling up capacity.

Conflicts of interest

There are no conflicts to declare.

Acknowledgements

The authors acknowledge the support of NSFC (81530057 and 81571746), the Taishan Scholar Program of Shandong Province of China (ts20110829) and CAS (2016YZ01).

Notes and references

1 N. Lee, D. Yoo, D. Ling, M. H. Cho, T. Hyeon and J. Cheon, *Chem. Rev.*, 2015, **115**, 10637–10689.

2 Z. Gao, T. Ma, E. Zhao, D. Docter, W. Yang, R. H. Stauber and M. Y. Gao, *Small*, 2016, **12**, 556–576.

3 J. Gao, H. Gu and B. Xu, *Acc. Chem. Res.*, 2009, **42**, 1097–1107.

4 Y. Jin, C. Jia, S. Huang, M. O'Donnell and X. Gao, *Nat. Commun.*, 2010, **1**, 1038–1042.

5 P. Cai, W. R. Leow, X. Wang, Y. Wu and X. Chen, *Adv. Mater.*, 2017, **29**, 1605529.

6 S. Sun, H. Zeng, D. B. Robinson, S. Raoux, P. M. Rice, S. X. Wang and G. Li, *J. Am. Chem. Soc.*, 2004, **126**, 273–279.

7 J. Park, E. Lee, N. M. Hwang, M. Kang, S. C. Kim, Y. Hwang, J.-G. Park, H. J. Noh, J. Y. Kim, J. H. Park and T. Hyeon, *Angew. Chem., Int. Ed.*, 2005, **117**, 2932–2937.

8 Q. Jia, J. Zeng, R. Qiao, L. Jing, L. Peng, F. Gu and M. Y. Gao, *J. Am. Chem. Soc.*, 2011, **133**, 19512–19523.

9 J. Huang, L. Bu, J. Xie, K. Chen, Z. Cheng, X. Li and X. Chen, *ACS Nano*, 2010, **4**, 7151–7160.

10 J. Zeng, L. Jing, Y. Hou, M. Jiao, R. Qiao, Q. Jia, C. Liu, F. Fang, H. Lei and M. Y. Gao, *Adv. Mater.*, 2014, **26**, 2694–2698.

11 J. Lynch, J. Zhuang, T. Wang, D. LaMontagne, H. Wu and Y. C. Cao, *J. Am. Chem. Soc.*, 2011, **133**, 12664–12674.

12 B. H. Kim, N. Lee, H. Kim, K. An, Y. I. Park, Y. Choi, K. Shin, Y. Lee, S. G. Kwon, H. B. Na, J. G. Park, T. Y. Ahn, Y. W. Kim, W. K. Moon, S. H. Choi and T. Hyeon, *J. Am. Chem. Soc.*, 2011, **133**, 12624–12631.

13 Z. Xu, C. Shen, Y. Hou, H. Gao and S. Sun, *Chem. Mater.*, 2009, **21**, 1778–1780.

14 M. Jiao, J. Zeng, L. Jing, C. Liu and M. Y. Gao, *Chem. Mater.*, 2015, **27**, 1299–1305.

15 M. Zhao, D. Ding, F. Yang, D. Wang, J. Lv, W. Hu, C. Lu and Z. Tang, *Nano Res.*, 2017, **10**, 1249–1257.

16 H. Zhang, L. Jing, J. Zeng, Y. Hou, Z. Li and M. Y. Gao, *Nanoscale*, 2014, **6**, 5918–5925.

17 N. R. Jana, Y. Chen and X. Peng, *Chem. Mater.*, 2004, **16**, 3931–3935.

18 M. Jiao, L. Jing, C. Liu, Y. Hou, J. Huang, X. Wei and M. Y. Gao, *Chem. Commun.*, 2016, **52**, 5872–5875.

19 Y. Wang, J. He, C. Liu, W. H. Chong and H. Chen, *Angew. Chem., Int. Ed.*, 2015, **54**, 2022–2051.

20 S. Marre and K. F. Jensen, *Chem. Soc. Rev.*, 2010, **39**, 1183–1202.

21 Q. Feng, J. Sun and X. Jiang, *Nanoscale*, 2016, **8**, 12430–12443.

22 P. Laurino, R. Kikkeri and P. H. Seeberger, *Nat. Protoc.*, 2011, **6**, 1209–1220.

23 S. Marre, J. Park, J. Rempel, J. Guan, M. G. Bawendi and K. F. Jensen, *Adv. Mater.*, 2008, **20**, 4830–4834.

24 E. M. Chan, A. P. Alivisatos and R. A. Mathies, *J. Am. Chem. Soc.*, 2005, **127**, 13854–13861.

25 D. Ness, J. Niehaus, V. H. Tran and H. Weller, *MRS Proc.*, 2012, **1386**, mrsf11-1386-d07-02.

26 Y. W. Jun, J. W. Seo and J. Cheon, *Acc. Chem. Res.*, 2008, **41**, 179–189.

27 D. Shi, M. E. Sadat, A. W. Dunn and D. B. Mast, *Nanoscale*, 2015, **7**, 8209–8232.